HHS Public Access

Author manuscript

Bioconjug Chem. Author manuscript; available in PMC 2018 September 08.

Published in final edited form as:

Bioconjug Chem. 2018 April 18; 29(4): 914–927. doi:10.1021/acs.bioconjchem.7b00816.

Filomicelles Deliver a Chemo-Differentiation Combination of Paclitaxel and Retinoic Acid That Durably Represses Carcinomas in Liver to Prolong Survival

Praful R. Nair, **Cory Alvey**, **Xiaoling Jin**, **Jerome Irianto**, **Irena Ivanovska**, and **Dennis E. Discher***

NanoBioPolymers Lab, and Physical Sciences Oncology Center @ Penn, University of Pennsylvania, Philadelphia, Pennsylvania 19104, United States

Abstract

Drug resistance and relapse is common in cancer treatments with chemotherapeutics, and while drug combinations with naturally occurring, differentiation-inducing retinoic acid (RA) provide remission-free cures for one type of liquid tumor, solid tumors present major problems for delivery. Here, inspired by filoviruses that can be microns in length, flexible filomicelles that self-assemble from an amphiphilic block copolymer (PEG−PCL) are shown to effectively deliver RA and paclitaxel (TAX) to several solid tumor models, particularly in the liver. These hydrophobic compounds synergistically load into the cores of the elongated micelles, and the coloaded micelles prove most effective at causing cell death, ploidy, and durable regression of tumors compared to free drugs or to separately loaded drugs. RA-TAX filomicelles also reduce mortality of human lung or liver derived cancers engrafted at liver, intraperitoneal, and subcutaneous sites in immunodeficient mice. In vitro studies show that the dual drug micelles effectively suppress proliferation while upregulating a generic differentiation marker. The results highlight the potency of dual-loaded filomicelles in killing cancer cells or else driving their differentiation away from growth.

Abstract

*Corresponding Author: discher@seas.upenn.edu.

Author Contributions

P.R.N., J.I., and D.E.D. designed the experiments. P.R.N. and J.I. carried out all experiments unless noted otherwise. X.J. established orthotopic liver models in vivo. C.A. assisted with experiments in Figures 4A, S4A, and S5D. P.R.N., C.A., J.I., and D.E.D. did the analysis and manuscript writing.

Supporting Information

The Supporting Information is available free of charge on the ACS Publications website at DOI: 10.1021/acs.bioconjchem.7b00816. Comparison of free and encapsulated RA; Treatments involving TAX; Quantification of total tumor burden in mice; Synergy between different drugs tested with free drug solutions; Dose response curves for free and filomicelle drug treatments (PDF)

The authors declare no competing financial interest.

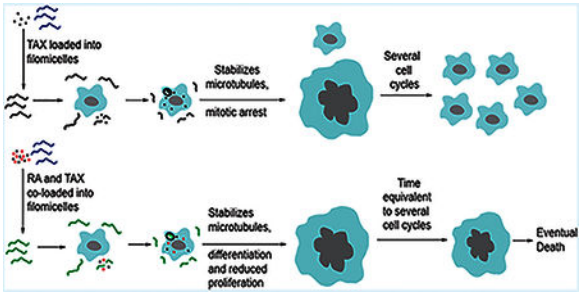

INTRODUCTION

Cancer cells are well-known to adapt to adverse conditions, with resistance emerging to drugs developed for cancer chemotherapy in part because of off-target toxicities that limit dosage[1] and also—for solid tumors—because of poor penetration.[2] Nanocarriers can sometimes greatly increase dosage, especially for poorly soluble drugs,[3] and they can also reduce off-target cytotoxicity,[4] but particles are generally cleared from circulation by phagocytes and thus less available for delivery of drugs. Inspired by elongated viruses such as highly infectious Ebola filovirus and some strains of Influenza virus, we have been studying the delivery capabilities of flexible and fragmentable “filomicelles”. They are self-assembled from amphiphilic block copolymers and intravenous injections show delayed clearance and enhanced delivery of hydrophobic drug to tumors compared to spherical micelles or to free drug—at least in the case of the hydrophobic drug paclitaxel.[5–7] Paclitaxel (TAX) is one of the most common chemotherapeutics in the clinic,[8] and functions by stabilizing microtubules, blocking mitosis, and inducing aneuploidy and/or cell death.[9,10] Being hydrophobic, dosage with free drug is low,[11] and filomicelles significantly increase loading and dosage[12] and can drive regression of subcutaneous solid tumors in vivo for weeks.[5] However, TAX-filomicelles have not been tested on tumors at clinically relevant disease sites (e.g., liver) nor on longer time scales, when drug resistance and relapse are more likely.

Relapse is commonly seen with conventional chemotherapy,[13] and one approach to reducing resistance is to use two drugs that act via orthogonal pathways.[14,15] Retinoic Acid (RA) is an attractive choice as a natural derivative of vitamin A that binds Retinoic Acid Receptors (RARs) (Figure 1A)[16–18] which regulate Retinoid Acid Response Elements (RARE) in DNA to ultimately control expression of differentiation programs,[19,20] including liver cells.[21,22] RA tends to reduce proliferation of cells by arresting the cell cycle in the G1 phase,[23,24] and one easily measured RA-regulated, generic marker of differentiation is nuclear lamin-A that encages the chromatin.[25] Although RARs are silenced in a few cancers,[26,27] RA is essential to life and provides a highly resilient cure for most cases (>90%) of acute promyelocytic leukemia (APL) when combined with chemotherapies.[28–29] However, APL is a liquid tumor, and RA plus TAX treatments of solid tumors have been tried with limited success for cancers of colon,[30] brain,[31] and breast,[32] as well as RA plus cisplatin in breast.[33] RA is normally stored in the liver within lipid droplets of stromal hepatic stellate cells,[34] and lower RA levels correlate with cancer-associated liver diseases such as cirrhosis[35] and Non-Alcoholic Fatty Liver Disease (NAFLD).[36,37] Indeed, in hepato-cellular carcinoma, hepatic

stellate cells lose RA, which leads to a general dedifferentiation and increased proliferation in the liver.[38] Restoring RA levels to normal in order to drive differentiation and arrest proliferation is thus especially attractive for liver carcinomas.[39] Although a phase II clinical trial with free RA plus TAX did not report significant benefit over TAX alone against breast carcinoma,[40] nanoparticle formulations of RA plus TAX are understudied. RA plus TAX filomicelles (Figure 1A) are therefore assessed here with the various needed comparisons in vitro and in vivo with several solid tumor models. We focus on liver cancer models, including metastatic liver disease (from lung, as is common) and primary liver cancer.

RESULTS

RA Arrests Carcinoma Proliferation and Drives Differentiation.

RA filomicelles suppress carcinoma cell growth at lower concentrations than free RA (Figure 1B) with an IC50 for RA filomicelles that is 200-fold more potent than free RA (Figure S1A). Empty filomicelles are inert at physiological concentrations with cell numbers close to that for untreated cell numbers. Kinetics of cell numbers treated with free and encapsulated RA shows that free RA requires 3 days for the antiproliferative effects (Figure S1B,C) whereas cell numbers for RA filomicelles begin to decrease within 2 days. Kinetics seem sensible relative to cell cycle and has been documented before.[25] Cell numbers with free RA at 50 μM are the same regardless of treatment time (1, 2, or 3 days) and suggests increased cell death at very high concentrations relative to typical pharmacological concentrations of ~1 μM.[28]

Arrested proliferation is reflected by a decrease in average DNA content per cell, due to a decreasing number of cells replicating DNA. DNA intensity indeed decreases monotonically with increasing concentrations of RA (Figure S1D). RA loaded filomicelles had an order of magnitude greater effect than free RA. DNA intensity histograms with free RA show suppression of the replication peak (Figure S1E,F). Fewer cells with twice the DNA content gives the decrease in average DNA intensity seen previously. The effect of RA filomicelles can be attributed to the drug alone as empty filomicelles do not appreciably alter the histogram (Figure S1F, inset). Back-calculation from cell numbers permits the estimation of percentage of cells differentiated (Figure S1G), which follows a Hill-type curve and reaches near maximum values after day 2 (Figure S1H), consistent with cell number kinetics. Back-calculation from the cell number data puts the proliferating fraction at ~5% (Figure S1G), based on simple binary state calculations in which the cell is assumed to either differentiate or be unaffected.

RA also induces differentiation and is a direct regulator of a generic marker of differentiation in the nucleus, Lamin-A.[25] RA-induced differentiation was therefore assessed through changes in Lamin-A levels. At low concentrations, RA decreases Lamin-A, but then increases at higher concentrations (Figure S2A). Untreated nuclei are rounded with uniform Lamin-A distribution on the edges. When treated with 10 μM RA as free drug, the nuclei become more elongated with patchy Lamin-A distribution. Nuclear aspect ratio increases monotonically with higher RA and then plateaus (Figure S2B), with the trend fitting a hyperbolic curve. Nuclear surface area and volume follow similar trends to Lamin-A (Figure S2C,E, respectively), and lamin-A levels normalized to either surface area or volume (Figure

S2D,F, respectively) increase linearly with RA. Higher levels of Lamin-A are suggestive of a more differentiated state, and since Lamin-A forms a meshwork at the periphery of the nucleus,[41] we normalized levels of Lamin-A to nuclear surface area (Figure S2D) to account for changes in nuclear size. To account for the decreased DNA content (which could globally decrease transcripts), Lamin-A was also normalized to volume (Figure S2F). Both quantities scaled linearly with RA concentration, indicating that the change in Lamin-A levels cannot be explained by changing nuclear geometry, consistent with RA transcriptionally altering levels of the protein. Nuclear geometry might, however, be able to explain the decrease in Lamin-A levels observed at low concentrations of RA. Lamin-A has been known to have a turnover rate that depends on matrix rigidity as does nuclear geometry.[42] Upon addition of RA, the resulting shrinkage in the nucleus (Figure S2C,E) might lead to excess Lamin-A per surface area, which might then be degraded. Most importantly in lamin-A regulation, RA-filomicelles were always an order of magnitude more effective than free drug.

RA-TAX Treatment Leads to Durable Reduction in in Vitro Relapse.

While single drugs fail to elicit a permanent response, with cells reverting to their quiescent state, the restoration of RA levels might differentiate the cell irreversibly, leading to a more durable treatment. This durability was assessed by a simple rescue experiment (Figure 1B), where cells were treated with drugs and incubated with fresh media post-treatment. The cells treated with RA consistently increase in number, and the difference in slopes indicate that a fraction of the cells exposed to RA have been differentiated and have lower proliferation. The slope decreases sharply from day 1 to day 2, consistent with the differentiation data (Figure S1G,H). Interestingly, there is little change in proliferation rate past day 2—even without further treatment. TAX treated cells decline in number initially, but cell death plateaus and then reverses after 1−2 weeks. Images show TAX-affected cells with massive nuclei among normal-looking cells. Such regrowth is observed frequently in vivo as well as in the clinic.[43,44] RA-TAX treated cells, on the other hand, consistently decrease in number, indicating a more durable treatment with all cells dying by ~4 weeks.

To clarify the influence of one drug on the other, we examined the hallmark of TAX treatment, which includes increased cell size and DNA accumulation, as measured by forward scatter and Hoechst intensity, respectively. Increased cell sizes for both TAX (1.5 times the untreated size) and RA-TAX (2.7 times the untreated size) were expected (Figures 1C, top, and S3A), but cell sizes for TAX treated cells returned to normal by day 9 (1.06-fold), whereas it remained high (at 3.1-fold) for RA-TAX treated cells after 29 days. Like cell size, DNA content (Figure 1C, bottom) was also increased for TAX (2.8 times relative to untreated) and RA-TAX (3.8). Like cell size, DNA content was back to normal after day 9 (1.09), while it was still high for RATAX treated cells after day 13 (5.8). By day 29, it had declined to 1.2, which combined with the increased cell size suggested that DNA synthesis was hindered after treatment. DNA content decreases for RA due to lower number of proliferating cells (0.7), but like TAX, it returned to normal (1.08) within 9 days. Normalization of DNA to area (Figure S3B) showed that cells treated with TAX (single drug or as a part of the combination) had the lowest values, suggesting that DNA synthesis might be affected after treatment. Histograms of DNA content (Figure S3C) shed further light on

the DNA content in surviving cells and confirmed that drug loaded filomicelles caused the highest ploidy.

Differences between separately loading RA and TAX (as was done previously) and loading both drugs together (coloading) were then assessed (Figure 1D). While there is no difference between the curves at very low or high concentrations, coloading filomicelles is ~4-fold more effective in terms of IC50s. Co-loaded drug is also ~10-fold more effective than free drugs.

A multiwell subcloning approach to in vitro “relapse” (Figure 1E) showed that nearly all cells treated with free TAX will relapse (>90%), which is consistent with the resistance suggested by Figure 1B. This rate is much lower for free RA-TAX treated cells (15%) at 3 weeks post-treatment, which indicates a much more durable response than just free TAX. TAX is susceptible to hydrolysis, reducing its activity,[45] and RA complexes tightly with albumin above 0.5% albumin,[46] so that loading these into nanocarriers could be protective. Indeed, while loading TAX into filomicelles still underscores the limitations of a single drug (Figure 1E, right), RA-TAX filomicelles show no relapses up to 4 weeks.

These in vitro studies thus illustrate the utility of drug combinations over single drugs (Figure 1B,C) and the potential benefits of a delivery system (Figure 1D,E) such as RA-TAX loaded filomicelles. These were therefore advanced to in vivo tests on carcinoma models with some of the needed controls for comparisons.

RA-TAX Filomicelles Durably Shrink Metastasis Model of Human Lung Derived Intraperitoneal and Subcutaneous Tumors in Mice.

Simple models of subcutaneous lung-derived A549 tumors were used to assess the in vivo efficacy of RA-TAX filomicelles before trying metastasis-type models. Free RA-TAX injections (TAX: 1.4 mg/kg, RA: 3 μg/kg) were administered via tail vein injections to NSG mice with sub-cutaneous A549 xenografts (Figure S4A). Four injections over the course of 11 days led to a modest regression of tumor size (15%) with the growth of the tumor arrested for ~3 weeks. To test filomicelles, mice with subcutaneous A549 xenografts were administered with a TAX dosage of 2.2 mg/kg and RA at 0.05 mg/kg (Figure S4B). As shown previously, RA-TAX filomicelles suppressed the growth of tumors, with effects lasting ~3−4 weeks after the last injection. The low RA dosage was evident in that the tumors failed to regress, but safety was evident with no decrease in mouse body weights with either of the above treatments (Figure S6A,B).

Mice bearing A549 intraperitoneal tumors as well as two subcutaneous tumors were treated with 4 injections of filomicelles with higher dose RA (0.35 mg/kg) and TAX (2 mg/kg) (Figure 2A). For both subcutaneous (Figure 2B) and intraperitoneal (Figure S4C) tumors, RA-TAX filomicelles produced the greatest tumor shrinkage (15% and 30%, respectively), and tumors remained small for ~3 weeks after treatment was stopped. Treated tumors started growing, but at a much slower rate than untreated tumors. It is likely that some cells in vivo do not receive sufficient drugs and continue to grow, which differs from the perfectly well-stirred delivery in cell culture (Figure 1B,E). Background colors indicate mouse survival, and both drug treatments extend survival compared to untreated (Figure S4D).

Single drugs alone could delay growth but failed to produce much shrinkage in any tumors. With intraperitoneal tumors, mice treated with single drugs showed resumption of tumor growth as soon as the treatment was terminated. Hence, for surviving mice treated initially with TAX filomicelles, the shorter first round of injections was followed by another round starting ~10 weeks later. By the beginning of the treatment, these tumors were growing at a rate similar to that of untreated tumors (gray curve). RA-TAX filomicelle injections produced an initial shrinkage in subcutaneous tumors, but the tumors soon resumed growth (Figure 2B). With intraperitoneal tumors, RA-TAX injection produced a brief retardation in growth but ultimately resumed growth at the same rate (Figure S4C), suggesting a maximum tumor size for the treatment to be effective. Durable tumor shrinkage by RA-TAX was evident in prolonged survival of RA-TAX treated mice (Figure S4D). TAX treated mice also displayed extended survival. RA treatment significantly improved lifespan compared to untreated ($p = 0.02$). However, subcutaneous tumor sizes measured by calipers 100 days after tumor treatment showed that RA-TAX tumors were 70% smaller than untreated ones (Figure S4D inset), and half the size of TAX treated tumors.

RA-TAX Filomicelles Extend Survival in Liver Meta-stasis Model of A549 Lung Carcinoma.

Intraperitoneal plus subcutaneous tumors of the lung cancer cells are not especially lethal, with untreated mice first succumbing at ~10 weeks, but lung cancers commonly metastasize to liver,[47,48] and of course ~90% of cancer related deaths occur due to metastasis.[49] Mice bearing liver A549 tumors (mimicking liver metastases) and subcutaneous tumors (for easy monitoring) were injected with filomicelles loaded with RA (0.35 mg/kg) and/or TAX (2 mg/kg) during an extended round of eight injections begun at 42 days. Untreated mice started to succumb at this point (~6 weeks).

RA-TAX filomicelles produced the greatest benefit on day 55 (Figure 3A), exhibiting the lowest tumor intensity for both liver and subcutaneous tumors. Dual drug filomicelles were again the most effective, initially shrinking tumors and then arresting tumor growth (for ~20 days) even after treatments were finished (Figures 3B,C, and S5A-C). Tumors grew with single drug controls, and untreated tumors more than doubled in size. Despite bearing liver tumors as well, the mice treated with RA-TAX show little loss in body weight (Figure S6C) while all other groups lost weight. The more effective treatment translated into the longest lifespan with RA-TAX filomicelles (Figure 3D). The extension in mean survival was about 70 days compared to untreated and 22 days more compared to TAX alone.

RA-TAX Filomicelles Shrink Orthotopic Liver Xeno-grafts of HepG2 Hepatoblastoma.

The efficacy of RA-TAX filomicelles was tested on subcutaneous xenografts established with a common liver carcinoma line, HepG2. RA-TAX filomicelle injections in mice with HepG2 subcutaneous tumors suppressed and then stabilized the tumor growth (Figure 4A), even though these studies used a lower dose of drugs compared to those above (TAX at 1.5 mg/kg and RA at 0.1 mg/kg). Untreated tumors more than tripled in size during the same time frame (3.2-fold from the start of treatment), and free RA-TAX had little effect on tumor growth (2.5-fold from the start of treatment). The dosage of RA and TAX was the same as from previous experiments. RA-TAX also reduced the growth rate of hepatocellular carcinoma cells, Huh7, as subcutaneous tumors (Figure S5D), producing a 25% decrease in

size at day 25 compared to untreated. Both treatments led to no loss in weight (Figure S6D,E).

To test the delivery potential of filomicelles to orthotopic liver tumors, mice were injected with HepG2 cells in the liver, and succumb within weeks if untreated. Liver tumors excised from mice treated with RA-TAX filomicelles were much smaller, and showed ~60% shrinkage compared to untreated (Figure 4B,C). Disaggregation of adjacent normal liver lobes showed a much larger population of cells stained positive for anti-human stain (2.2%) compared to RA-TAX filomicelles (0.9%) treated, and this is evident in the histogram of anti-human stain intensities (Figure 4C, Figure S5E). Similar reduction in tumor volume and in HepG2 cells in adjacent lobes (~60% each) implies efficacy of filomicelles in delivering drugs throughout the liver and not just to the tumor regions. RA-TAX filomicelles indeed prolonged the survival of treated mice ($p = 0.02$) (Figure 4D), while no signifi-cant extension was seen with free RA-TAX. Nanocarriers thus maximize delivery.

The various in vitro and in vivo findings demonstrate increased durability of RA-TAX filomicelle treatments over current free drug chemotherapeutics. A survival benefit is also evident with RA-TAX filomicelle treatments of models of human liver tumors, including both a lung tumor metastatic model and liver cancer cell lines. Potential mechanisms were therefore examined more deeply.

RA Synergizes Better with Paclitaxel than with DNA Damaging Chemotherapeutics.

Three chemotherapeutics (Paclitaxel, Oxaliplatin, and 5-Fluorouracil) were combined with RA and the cell viabilities were studied on an EC4 mouse liver carcinoma line to identify the best drug combination with RA (Figure S7A-C). IC50 values from the cell viability curves (Figure 5A) show paclitaxel has the largest improvement upon the addition of RA (more than a 2.5-fold decrease from free TAX), while the IC50 of Oxaliplatin was reduced 1.5-fold. Addition of RA had minimal effect on the potency of 5-fluorouracil. To evaluate a sample combination chemotherapy, we investigated the combination of Paclitaxel (TAX) and 5-Fluorouracil (5FU) on A549 cells (Figure S7D). Combination of the two drugs were not as potent as TAX, as indicated by a rightward shift. They were however more effective than 5FU. Furthermore, the potency of the combination was dictated by TAX content, i.e., mixtures with higher amount of TAX were more successful than those having higher 5FU. This pointed to the lack of synergy between the two drugs, and IC50 values (Figure S7E bargraph) underscored this conclusion.

The optimal drug ratio of the TAX-RA combination was then sought (Figure S7F), using the A549 cells and three molar ratios: 3:100, 1:100, and 1:300 (TAX:RA). All combinations were found to be more potent than either single drug. 1:100 had the lowest IC50 (3 nM; Figures 5B, S7G), ~30-fold lower than free TAX (95 nM). The other two combinations had comparable IC50s (15 and 18 nM), despite an order of magnitude difference in TAX content. RA was relatively inert with an IC50 of 72 μM. The molar ratio of 1:100 between TAX and RA was thus optimal, and the efficacy of the combination on two different cell lines of different origins further underlines its potency.

Co-Loaded RA-TAX Filomicelles Are Most Potent, But Resistant Cells Emerge with Slow Proliferation.

When loaded into filomicelles, RA, TAX, or RA-TAX had a lower IC50 for counts of EC4 cells than free drugs (Figures 5C, S8A). RA-TAX filomicelles were 3-fold more potent than free drugs as were TAX filomicelles when compared to free TAX, but RA gains were greatest. Empty filomicelles were inert at relevant concentrations, although amphiphilic diblock copolymers can destabilize the lipid membrane at high concentration. Consistent with these results were separate findings from flow cytometry and trypan blue exclusion for cell survival and death, respectively (Figure S8B,C), and the relatively high cell densities on plates with any form of RA supports the mechanism of differentiation relative to TAX-induced cell death. Cell viabilities after days 1 and 3 with RA-TAX (Figure S8D,E) show that filomicelles are always more effective than free drug, but both treatments show increased potency with time. Cells incubated with empty filomicelles did not show any abnormal nuclear morphology when stained for nuclear lamin-A (Figure 5D, top), but RA caused elongation (Figure S2B), and TAX or RA-TAX led to massive blebbed nuclei (Figure 5D, bottom), a hallmark of TAX treatments.

In conducting these functional studies of drug synergy, we noted that RA integrates efficiently regardless of TAX, but that loading efficiencies of TAX were higher with coloaded filomicelles than when separately loaded (Figure S9A,B). Loading of TAX in PEG −PCL micelles has been extensively studied even in molecularly detailed simulation,[12] and the highly conjugated aliphatic chain of RA (terminating in −COOH) is likely compatible with the aromatic and oxygen-rich nature of TAX. Such synergistic interactions within micellar cores could be functionally important to drug release mechanisms and bioactivity—which would be best motivated by efficacy that is the focus of this study.

Cell colonies acquiring resistance to RA-TAX filomicelles were isolated and expanded to measure doubling times (Figure 5E). Resistant cells have higher doubling time (slower replication) than EC4 control cells (Figure S9C), with more resistant cells displaying a higher IC50 than normal EC4 cells (Figure S9D). From this data, the degree of resistance was calculated (Figure 5E), and a plot of proliferation rate against the degree of resistance displayed an anticorrelation (Figure 5F). The colony with the slowest replication rate (denoted as “RTMR2”) had the highest fraction of resistant cells. Untreated EC4 cells had the fastest replication and lowest resistant fraction, but all other clones lay on a line between these two extremes.

Cells were disaggregated from subcutaneous TdA549 tumors that were untreated, RA, and RA-TAX worms treated (mice from Figure 2 and S4C). Free RA-TAX dose responses were checked for all 3 groups as well as TdA549s in culture. All curves cluster close together (Figure S9E), with none of the IC50s being significantly different (Figure S9F). Based on Figure 5F, cells surviving RA-TAX treatment displayed increased IC50 to subsequent RA-TAX treatments, and this resistance is heritable after ~250 cell cycles. This helps clarify the apparent discrepancy between in vitro and vivo results. While RA-TAX halts proliferation in vitro, tumors treated in vivo invariably start growing after treatment is halted. The lack of observed resistance in cells disaggregated from RA-TAX treated tumors might be due to the lack of drug uptake, possibly due to inefficient angiogenesis.

Generic Differentiation Marker, Lamin-A, Increases While Proliferation Markers Increase with RA-TAX.

Levels of lamin-A normalized to DNA content increased with drug treatments for RA and moreso for RA-TAX, with both free drug and drug-loaded filomicelles (Figures 6A and S10A). RA-TAX filomicelles had the maximum effect of 3.6-fold up-regulation of lamin-A relative to untreated and free RA had the lowest (1.3-fold). Flow cytometry scatterplots of Lamin-A versus DNA confirm the population shifts toward those cells staining high while also illustrating the heterogeneity (Figure S10B).

Compared to differentiation and relative to untreated cells, proliferation markers and Cyclin D1 both showed the opposite trends with RA and RA-TAX (Figure 6B,C)—even with the greatly increased cell size and DNA content (Figure 1C). Images of cells treated with TAX or with RA-TAX reveal larger nuclei (Figure 6D), but cells treated with TAX alone still stain positive for Ki-67 unlike RA-TAX treated cells. Filomicelles further suppress these low signals (Figure 6E), and flow cytometry histograms confirm a large fraction of cells negative for Cyclin D1 an Ki67 levels after free drug treatment but especially with filomicelles (Figure 6F,G, respectively). Flow scatter-plots of Ki-67 versus DNA and Cyclin D1 versus DNA confirm population shifts toward cells with higher DNA and lower proliferation proteins (Figure S10C,D).

Potency of RA-TAX Treatment Extends to Other Carcinomas and Sarcomas.

The efficacy of RA-TAX on c-myc driven mouse EC4 liver cancer cells might be representative of its effect on other aggressive tumors, and a central role of RA in liver carcinogenesis suggest particular applicability to other liver cancer lines. With the human Huh7 cell line, the combination was found to be more effective than either of the free drug alone (Figure S11A, RA-TAX IC50:3 nM, TAX IC50:13 nM), despite a lack of responsiveness to RA alone (IC50:5 μM). Further tests on A549 carcinoma as well as the sarcoma lines U2OS and RH30 confirm the promise of the approach (Figure S11B−D): RATAX filomicelles exhibit a much lower IC50 (1 nM) than TAX filomicelles (25 nM) in A549 cells, and this trend was repeated with U2OS (RA-TAX IC50:3 nM, TAX IC50:8 nM) and RH30 cells (RA-TAX IC50:1 nM, TAX IC50:4 nM). Dose responses of all cell lines to free drugs likewise reveal higher efficacy of free RA-TAX over single drugs (Figure S7).

Safety Tests on Normal Cells.

While the RA-TAX combination shows robust suppression of tumor growth (Figures 2B, 3B, and 4A), the Kaplan−Meier curves show that survival is not proportionately prolonged even though the effect is highly significant (Figures 3D and4D). Toxicity is one possibility, and so to begin to assess broader safety aspects, we used mesenchymal stem cells (MSCs), which are slow cycling cells found in nearly every tissue in perivascular niches, including liver where they are called hepatic stellate cells.[34] We specifically used MSCs derived from induced pluripotent stem cells (iPS cells) as a reproducible and generic source of these normal karyotype cells.[50,51] We find that RA suppresses iPS-MSC cell numbers only at ~1 mM, which is far above the doses that affect more rapidly cycling carcinoma cells (Figure 7A). We have recently shown RA suppresses Lamin-A expression in the iPS-MSCs,[51] which also differs from the observations here of the carcinoma cells (Figure 6D). RA is a natural

metabolite of vitamin-A, and so—unlike TAX—normal cells are constantly exposed to RA (~10 nM is physiological).[52] On the other hand, TAX (at 10 nM) blocks proliferation (including Ki-67) of iPS-MSC cell numbers as effectively as carcinoma cells, although viability of the latter is clearly compromised (Figure 7B). These in vitro results thus indicate unsurprisingly that TAX in the RA-TAX combination exerts effects on normal cells that are slowly cycling, and so TAX is therefore a likely source of systemic toxicity.

DISCUSSION

RA is an essential derivative of vitamin A that does not induce cell death at typical pharmacological concentrations (~1 μM) but does arrest proliferation and drive differentiation. DNA damaging agents can also delay progression through cell cycle and cause apoptosis, but RA might antagonize by promoting DNA repair.[53] TAX stabilizes microtubules and impedes cell cycle more specifically at the metaphase-anaphase transition, leading to bigger blebbed nuclei that can still differentiate (Figures 5D and6D). However, consistent with our own observations that free RA-TAX provides minimal benefit (Figures 4A and S4A,B), RA-TAX showed no benefit relative to TAX in a phase II trial with breast cancer patients.[40] Evidence of higher rates of stable disease in treated patients is also consistent with the differentiating, anti-proliferative effects of RA, and so we hypothesized that better efficacy could be achieved with better delivery. Our in vivo experiments show RA-TAX-filomicelles are the most potent and durable means of delivery. The higher efficiency of coloaded filomicelles (Figure 1D) further suggests that the simultaneous presence of both RA and TAX is beneficial, perhaps ensuring adequate delivery of both compounds to the same cell at the same time. Other synergistic combinations might likewise be improved with nanobased delivery. Interestingly, others have shown that filamentous nanostructures such as those of peptide conjugates have reduced cellular uptake compared to free drug in vitro.[54] However, our lab has previously shown that uptake can lead to a “depot effect” with more drug in a cell at a critical time (e.g., mitosis) compared to free drug.[6]

RA-filomicelles cause a 3-fold increase in lamin-A protein levels compared to 1.3 for free RA, which supports the hypothesis that loading RA into filomicelles protects it from complexation with albumin, and thereby increases its efficacy. Lamin-B is not as responsive to RA as Lamin-A.[56] Resistance to RA-TAX is favored by slow proliferation (Figure 5F), consistent with drug resistance impeding cell proliferation.[55] In the studies here, resistant colonies were expanded for about 200−250 cell cycles and thus given sufficient time to recover from the stress of exposure to drugs (Figure 5E), and so acquired resistance was not transient. Such resistant cells might be outcompeted by faster proliferating cells that are less resistant and that might be treated again. A similar rationale has been used to develop competitive therapies such as “evolutionary double bind therapy”,[56] which could one day be an integral part of chemotherapy.

Extension of durability of RA-TAX treatments to in vivo models was done with various xenografts in an immunodeficient NOD-SCID strain of mouse. Although RA can affect differentiation of immune cells, which is the basis for success of chemo-differentiation for liquid tumors of APL,[57] reasonable success here on mice with solid liver tumors seems promising. Untreated mice exhibited a high mortality rate, unlike NSG mice with only

subcutaneous tumors, and the effects likely reflect compromised liver function, leading to shutdown of vital processes.[58] Efficacy against cancer cells derived from tissues outside the liver suggest that the function of RA is common to many cells, with RARs and RAREs regulating many key differentiation processes in diverse tissues.

CONCLUSIONS

A goal of this study was to highlight two key advances over conventional chemotherapy. First, chemo-differentiation therapy can be highly beneficial relative to single drug treatments or combination of chemotherapeutics. Second, nanocarriers can greatly increase efficacy of delivery, and perhaps shields integrated drugs from off-target interactions (such as RA with albmin). RA and TAX in filomicelle nanocarriers ultimately illustrate a more durable treatment than current formulations.

MATERIALS AND METHODS

Experimental Design.

All experiments were replicated ($n = 3$ or more). Measurements and analysis, when applicable, were conducted blindly with stratified sampling. In the case of tumor growth and regression studies, mice were not stratified, but separated by tumor size to ensure all groups had the same average tumor size at the start of treatment. No data was excluded from any data set.

Materials.

All chemical reagents were purchased from Sigma-Aldrich Corp., St. Louis, Missouri, unless stated otherwise. Ham's F-12 growth media, FBS, penicillin−streptomycin, nonessential amino acids, and MTT assay were purchased from Invitrogen. Hoechst 33342 was purchased from ThermoFisher (H3570). High glucose DMEM growth media was purchased from Corning. Dispase was purchased from StemCell Technologies (7913). Lamin-A (4C11), Cyclin D1, and Ki67 antibodies were purchased from Cell Signaling.

Synthesis of PEG−PCL and Characterization of Aggregates.

Polyethylene glycol (PEG)−Polycaprolactone (PCL) diblock copolymer was prepared as described previously.[59] Briefly, the diblock copolymer was prepared by the ring-opening polymerization of ε-caprolactone using PEG_{2000} as macroinitiator at 140 °C in the presence of stannous octoate as catalyst. The polymer was characterized by ^{1}H NMR spectroscopy and Gel Permeation Chromatography (GPC). Filomicelles were formed in water, imaged, and loaded with drug as described in ref 59.

Cell Culture.

A549 human lung cancer (CCL-185), Huh7 human liver cancer, HepG2 Human hepatocellular carcinoma (HB-8065), and U2OS human bone sarcoma (HTB-96) cell lines were purchased from ATCC and grown as per standard ATCC cell culture protocol. Primary EC4 mouse liver cancer cell line (c-myc mutation) was acquired from Chi Van Dang's lab at the University of Pennsylvania and cultured with DMEM High glucose growth media (4.5

g/L glucose with L-glutamine and sodium pyruvate) supplemented with 10% FBS, 1% penicillin− streptomycin, and 1% nonessential amino acids at 37 °C and 5% CO_2. When the flasks were confluent, the cells were passaged by dissociation with 0.05% Trypsin-EDTA (Invitrogen) and replated with fresh media at a confluency of 10%.

In Vitro Cell Viability Assay.

In vitro cytotoxicity assay was performed as described in ref 59. Briefly, 5000 cells were seeded in 96-well plates and treated with different drug concentrations the next day. After 3 days of incubation, the media was aspirated, and cells were incubated with media and MTT solution (5 mg/mL in PBS) for 3 h. The MTT formazan crystals were dissolved in DMSO, and absorbance was measured at 550 nm. Additional cell death quantification was done by counting the number of floating cells staining positive for Trypan Blue stain.

Rescue Experiments to Determine RA-TAX Durability.

50,000 cells were plated in 6-well plates and allowed to adhere for 24 h. After 1 day, the media was exchanged with fresh media and cells were incubated with free RA-TAX combination (1 μM and 10 nM) or PBS (negative control). Free RA (1 μM) and free TAX (10 nM) were the positive controls. After the 3 day incubation, the drug containing media was aspirated, wells were washed with PBS, and surviving cells were incubated with fresh media. The media was then replaced with fresh media twice a week until the cells were analyzed by flow cytometry. At fixed time intervals, 3 wells of each control as well as treatment group were detached from the plate by trypsinizing, stained for DNA (with Hoechst 33342 solution (0.01% of 10 mg/mL solution in water) for 5 min and analyzed by flow cytometry to record cell number.

In Vitro “Relapse” Studies.

As with cell viability studies, 5000 cells were seeded in 96-well plates, with each well representative of a tumor. As was done with the above-mentioned durability studies, cells were treated with different formulations (free RA-TAX, free TAX, TAX loaded filomicelles, or RA-TAX loaded filomicelles) for 3 days, after which media was washed out and cells were incubated with fresh media. The cell numbers were monitored in each well, as were the number of wells with a resistant colony. For every time point, the number of wells with a resistant colony were recorded and a plot of percentage of wells relapsed vs time was plotted.

Cell Fixing and Immunofluorescence.

Cells in 6-well plates were treated with drugs as indicated above. After the desired time-point, cells were fixed using 4% paraformaldehyde for 10 min followed by 3 PBS washes. Cells were then permeabilized with 0.5% Triton-X for 10 min, followed by 3 PBS washes. After 30 min of blocking with 5% BSA, the cells were incubated overnight with the primary antibody at 4 °C. The next day, the cells were incubated with secondary antibody at room temperature for 1.5 h and then washed 3 times with PBS. The cells were then stained with Hoechst 33342 solution (0.01% of 10 mg/mL solution in water) for 10 min, followed by 3 more washes with PBS. The cells were fixed again and stored in PBS at 4 °C. The stained

cells were visualized under an Olympus IX71 microscope with a 300 W xenon lamp using 40× objective (0.60 NA). Images were analyzed by ImageJ software (NIH).

Intracellular Protein Staining and Flow Cytometry Analysis.

The cells were detached with 0.05% Trypsin, spun down, and washed with PBS. They were fixed with 1.6% paraformaldehyde for 10 min and permeabilized with 0.1% saponin for 10 min. The cells were then spun down, resuspended with the conjugated antibodies, and incubated for 1.5 h and stained for DNA with Hoechst 33342 solution (0.01% of 10 mg/mL solution in water) for 5 min. After this incubation, cells were spun down and suspended in flow buffer (5% FBS in PBS). Cells were run through a flow cytometer (BD LSR II) and data was analyzed by WEASEL v 3.2.1 software.

Establishment of Xenograft Model for Liver Metastasis of Tumor.

All animal experiments were approved by Institutional Animal Care and Use Committee of the University of Pennsylvania and in accordance with NIH publication No. 86−23. Eight- to ten-week-old NOD-SCID-IL-2Rgc null mice (NSG) were purchased from the Stem Cell and Xenograft Core of University of Pennsylvania (Philadelphia, PA) and housed in a specific-pathogen-free facility. Mice were anesthetized using 4% isoflurane in 3 L/min O_2, after which isoflurane percentage was maintained 2%. To examine the therapy for liver metastasis of tumor, 10^6 of A549 human lung cancer cells labeled with td-Tomato were injected into the murine liver. Briefly, the anesthetized mouse was placed supine, maintaining inhalational isoflurane anesthesia (2% (v/v) in 2 L/min O_2) with a nose cone. For analgesia, buprenorphine SR (1 mg/kg, ZooPharm, Fort Collins, CO) was subcutaneously injected on the animal's flank. The skin was shaved and the skin on the ventral abdomen and partial thorax was sterilized with chlorhexidine swab (Professional Disposables International, Inc. Orangeburg, NY. Cat. # B10800). Using sterile sharp scissors (Roboz Surgical Instrument Co., Inc. Gaithersburg, MD. cat. # RS-5916), a 15 mm of midline abdomina incision was made and the linea alba was opened to enter the peritoneal cavity. 25 μL of tumor cells suspension (10^6 /25 μL of 25% Matrigel in PBS) was loaded into an insulin syringe with 30 G 1/2-in. needle (MHC Medical Products, LLC, Fairfield, Ohio, cat. # 08496-3035-11). The left lateral lobe of the liver was then exposed using forceps (Roboz Surgical Instrument Co., Inc. Gaithersburg, MD. cat. # RS-8254). The liver was stabilized with a cotton-tip applicator (Fischer Scientific, cat. # 23-400-125), and the syringe was positioned inserting the needle into the liver and advancing the tip along the subserosal plane for a few millimeters. The tumor cell suspension in the syringe was gently discharged and the needle was removed from the liver. The puncture site was gently pressed with a cotton-tipped applicator to prevent leakage of the tumor cell suspension and to achieve complete hemostasis. Finally, the incision was closed with an absorbable 4−0 sutures (Ethicon Inc. Somerville, NJ. cat. # VR494).

In Vivo Subcutaneous Xenografts and Treatment.

An A549 cell line expressing td-Tomato was dissociated from tissue culture flasks using 10 mM trypsin in PBS. For each injection, 10^6 or 2×10^6 cells were suspended in 100 μL ice-cold PBS and 25% Matrigel (BD) and injected subcutaneously into the flank or intraperitoneal of nonobese diabetic/severe combined immunodeficient (NOD/SCID) mice

with null expression of interleukin-2 receptor gamma chain (NSG mice). All other xenografts using different cell lines were made using this protocol. RA-Paclitaxel loaded filomicelles were administered using tail vein injection (250 μL per injection). The treatment consisted of four, six, or eight injections each, administered in regular intervals over 2 to 3 weeks. Tumor size was measured at regular intervals using calipers. The tumor area was normalized to tumor size at the start of treatment. Caliper measurements (for subcutaneous tumors) as well as mouse body weight were recorded twice a week.

In Vivo Tumor Imaging.

Mice were anesthetized via inhalation of isoflurane at 3 L/min and maintained at 1.5 L/min. Images were acquired using a PerkinElmer IVIS Spectrum with excitation and emission filters set at 535 and 580 nm, respectively, optimized for tdTom imaging. Images of each face of the sagittal plane were taken to capture both left and right flanks. Mouse fur was soaked with ethanol to reduce auto fluorescence prior to imaging. Three fluorescent standards were used to subtract background fluorescence and calibrate IVIS. Images were analyzed in ImageJ, where the length and width of the tdTom tumor was measured. Analysis of tdTom intensity was done using Living Image (PerkinElmer), which involved spectral unmixing of 10−13 images to sufficiently remove any tdTom autofluorescence from the mice.

Tumor Disaggregation and Anti-Human Staining.

After the mice were euthanized, the tumors were excised and diced into pieces no larger than 1 mm^3. These chunks were then incubated with digestion buffer (containing 9 mg collagenase (Sigma, C0130−100MG), 3 mL Dispase at 5 U/mL and 200 μL of 1 mg/mL DNase I (Sigma, 11284932001) solution) for 20 min at 37 °C. The digested mix was passed through a 70 μm filter and washed with 10 mL of PBS. The filtrate was spun down to obtain a cell pellet. Any RBC present were lysed with RBS lysis buffer (sigma, R7757). Cells were Fc blocked with CD32/CD16 (BD Pharmingen, clone 2.4G2, 553141) antibody for 10 min to prevent nonspecific staining. The cells were then incubated with primary and secondary antibodies for 30 min each. The cells were then washed with 5% FBS, stained with Hoechst (10 min), and run through a flow cytometer (BD LSR II).

Curve Fitting and Statistical Analyses.

All curve fitting and data analysis was performed with OriginPro 8 software. Unless indicated otherwise, mean and standard deviation are calculated for a minimum of $n = 3$ independent samples.

Supplementary Material

Refer to Web version on PubMed Central for supplementary material.

ACKNOWLEDGMENTS

Support from the NIH (U54-CA193417, R01-HL124106) and the National Science Foundation (DMR-1120901 to Penn's Materials Research Science and Engineering Center) is gratefully acknowledged. Animal imaging was

performed at the University of Pennsylvania Small Animal Imaging Facility (SAIF) Optical/Bioluminescence Core, supported by NIH grant CA016520.

REFERENCES

(1). Chidambaram M, Manavalan R, and Kathiresan K (2011) Nanotherapeutics to overcome conventional cancer chemotherapy limitations. J. Pharm. Pharm. Sci 14, 67–77. [PubMed: 21501554]

(2). Tredan O, Galmarini CM, Patel K, and Tannock IF (2007) Drug resistance and the solid tumor microenvironment. Journal of the National Cancer Institute 99, 1441–54. [PubMed: 17895480]

(3). Kipp JE (2004) The role of solid nanoparticle technology in the parenteral delivery of poorly water-soluble drugs. Int. J. Pharm 284, 109–22. [PubMed: 15454302]

(4). De Jong WH, and Borm PJ (2008) Drug delivery and nanoparticles:applications and hazards. Int. J. Nanomed 3, 133–49.

(5). Christian DA, Cai S, Garbuzenko OB, Harada T, Zajac AL, Minko T, and Discher DE (2009) Flexible filaments for in vivo imaging and delivery: persistent circulation of filomicelles opens the dosage window for sustained tumor shrinkage. Mol. Pharmaceutics 6, 1343–52.

(6). Geng Y, Dalhaimer P, Cai S, Tsai R, Tewari M, Minko T, and Discher DE (2007) Shape effects of filaments versus spherical particles in flow and drug delivery. Nat. Nanotechnol 2, 249–55. [PubMed: 18654271]

(7). Rajagopal K, Mahmud A, Christian DA, Pajerowski JD, Brown AE, Loverde SM, and Discher DE (2010) Curvature-coupled hydration of Semicrystalline Polymer Amphiphiles yields flexible Worm Micelles but favors rigid Vesicles: polycaprolactone-based block copolymers. Macromolecules 43, 9736–9746. [PubMed: 21499509]

(8). Wall ME (1998) Camptothecin and taxol: discovery to clinic. Med. Res. Rev 18, 299–314. [PubMed: 9735871]

(9). Jordan MA, Wendell K, Gardiner S, Derry WB, Copp H, and Wilson L (1996) Mitotic block induced in HeLa cells by low concentrations of paclitaxel (Taxol) results in abnormal mitotic exit and apoptotic cell death. Cancer Res 56, 816–25. [PubMed: 8631019]

(10). Long BH, and Fairchild CR (1994) Paclitaxel inhibits progression of mitotic cells to G1 phase by interference with spindle formation without affecting other microtubule functions during anaphase and telephase. Cancer Res 54, 4355–61. [PubMed: 7913875]

(11). Zhang X, Burt HM, Von Hoff D, Dexter D, Mangold G, Degen D, Oktaba AM, and Hunter WL (1997) An investigation of the antitumour activity and biodistribution of polymeric micellar paclitaxel. Cancer Chemother. Pharmacol 40, 81–6. [PubMed: 9137535]

(12). Loverde SM, Klein ML, and Discher DE (2012) Nanoparticle shape improves delivery: rational coarse grain molecular dynamics (rCG-MD) of taxol in worm-like PEG-PCL micelles. Adv. Mater 24, 3823–30. [PubMed: 22105885]

(13). Komarova NL, and Wodarz D (2005) Drug resistance in cancer: principles of emergence and prevention. Proc. Natl. Acad. Sci. U. S. A 102, 9714–9. [PubMed: 15980154]

(14). Deng GL, Zeng S, and Shen H (2015) Chemotherapy and target therapy for hepatocellular carcinoma: New advances and challenges. World journal of hepatology 7, 787–98. [PubMed: 25914779]

(15). Bokemeyer C, Oechsle K, Honecker F, Mayer F, Hartmann JT, Waller CF, Bohlke I, Kollmannsberger C, and German Testicular Cancer Study, G (2008) Combination chemotherapy with gemcitabine, oxaliplatin, and paclitaxel in patients with cisplatin-refractory or multiply relapsed germ-cell tumors: a study of the German Testicular Cancer Study Group. Annals of oncology: official journal of the European Society for Medical Oncology 19, 448–53. [PubMed: 18006893]

(16). Theodosiou M, Laudet V, and Schubert M (2010) From carrot to clinic: an overview of the retinoic acid signaling pathway. Cell. Mol. Life Sci 67, 1423–45. [PubMed: 20140749]

(17). Mark M, Ghyselinck NB, and Chambon P (2006) Function of retinoid nuclear receptors: lessons from genetic and pharmacological dissections of the retinoic acid signaling pathway during mouse embryogenesis. Annu. Rev. Pharmacol. Toxicol 46, 451–80. [PubMed: 16402912]

(18). Leid M, Kastner P, and Chambon P (1992) Multiplicity generates diversity in the retinoic acid signalling pathways. Trends Biochem. Sci 17, 427–33. [PubMed: 1333659]

(19). Wu H, Zhang G, Minton JE, Ross CR, and Blecha F (2000) Regulation of cathelicidin gene expression: induction by lipopolysaccharide, interleukin-6, retinoic acid, and Salmonella enterica serovar typhimurium infection. Infection and immunity 68, 5552–8. [PubMed: 10992453]

(20). Lawson ND, and Berliner N (1999) Neutrophil maturation and the role of retinoic acid. Exp. Hematol 27, 1355–67. [PubMed: 10480426]

(21). Huang J, Bi Y, Zhu GH, He Y, Su Y, He BC, Wang Y, Kang Q, Chen L, Zuo GW, et al. (2009) Retinoic acid signalling induces the differentiation of mouse fetal liver-derived hepatic progenitor cells. Liver Int 29, 1569–81. [PubMed: 19737349]

(22). Breitman TR, Selonick SE, and Collins SJ (1980) Induction of differentiation of the human promyelocytic leukemia cell line (HL-60) by retinoic acid. Proc. Natl. Acad. Sci. U. S. A 77, 2936–40. [PubMed: 6930676]

(23). Zhu WY, Jones CS, Kiss A, Matsukuma K, Amin S, and De Luca LM (1997) Retinoic acid inhibition of cell cycle progression in MCF-7 human breast cancer cells. Exp. Cell Res 234, 293–9. [PubMed: 9260897]

(24). Collins SJ (1987) The HL-60 promyelocytic leukemia cell line: proliferation, differentiation, and cellular oncogene expression. Blood 70, 1233–44. [PubMed: 3311197]

(25). Swift J, Ivanovska IL, Buxboim A, Harada T, Dingal PC, Pinter J, Pajerowski JD, Spinler KR, Shin JW, Tewari M, et al. (2013) Nuclear lamin-A scales with tissue stiffness and enhances matrix-directed differentiation. Science 341, 1240104. [PubMed: 23990565]

(26). Connolly RM, Nguyen NK, and Sukumar S (2013) Molecular pathways: current role and future directions of the retinoic acid pathway in cancer prevention and treatment. Clin. Cancer Res 19, 1651–9. [PubMed: 23322901]

(27). Virmani AK, Rathi A, Zochbauer-Muller S, Sacchi N, Fukuyama Y, Bryant D, Maitra A, Heda S, Fong KM, Thunnissen F, et al. (2000) Promoter methylation and silencing of the retinoic acid receptor-beta gene in lung carcinomas. Journal of the National Cancer Institute 92, 1303–7. [PubMed: 10944551]

(28). Jing Y, Wang L, Xia L, Chen GQ, Chen Z, Miller WH, and Waxman S (2001) Combined effect of all-trans retinoic acid and arsenic trioxide in acute promyelocytic leukemia cells in vitro and in vivo. Blood 97, 264–9. [PubMed: 11133770]

(29). Soignet SL, Maslak P, Wang ZG, Jhanwar S, Calleja E, Dardashti LJ, Corso D, DeBlasio A, Gabrilove J, Scheinberg DA, et al. (1998) Complete remission after treatment of acute promyelocytic leukemia with arsenic trioxide. N. Engl. J. Med 339, 1341–8. [PubMed: 9801394]

(30). Hong GY, Jeong YI, Lee SJ, Lee E, Oh JS, and Lee HC (2011) Combination of paclitaxel- and retinoic acid-incorporated nanoparticles for the treatment of CT-26 colon carcinoma. Arch. Pharmacal Res 34, 407–17.

(31). Karmakar S, Banik NL, and Ray SK (2008) Combination of all-trans retinoic acid and paclitaxel-induced differentiation and apoptosis in human glioblastoma U87MG xenografts in nude mice. Cancer 112, 596–607. [PubMed: 18098270]

(32). Pratt MA, Niu MY, and Renart LI (2006) Regulation of survivin by retinoic acid and its role in paclitaxel-mediated cytotoxicity in MCF-7 breast cancer cells. Apoptosis 11, 589–605. [PubMed: 16528475]

(33). Zhang Y, Guan DX, Shi J, Gao H, Li JJ, Zhao JS, Qiu L, Liu J, Li N, Guo WX, et al. (2013) All-trans retinoic acid potentiates the chemotherapeutic effect of cisplatin by inducing differentiation of tumor initiating cells in liver cancer. J. Hepatol 59, 1255–63. [PubMed: 23867314]

(34). Blaner WS, O'Byrne SM, Wongsiriroj N, Kluwe J, D'Ambrosio DM, Jiang H, Schwabe RF, Hillman EM, Piantedosi R, and Libien J (2009) Hepatic stellate cell lipid droplets: a specialized lipid droplet for retinoid storage. Biochim. Biophys. Acta, Mol. Cell Biol. Lipids 1791, 467–73.

(35). Lee YA, Wallace MC, and Friedman SL (2015) Pathobiology of liver fibrosis: a translational success story. Gut 64, 830–41. [PubMed: 25681399]

(36). Liu Y, Chen H, Wang J, Zhou W, Sun R, and Xia M (2015) Association of serum retinoic acid with hepatic steatosis and liver injury in nonalcoholic fatty liver disease. Am. J. Clin. Nutr 102, 130–7. [PubMed: 25948673]

(37). Kim SC, Kim CK, Axe D, Cook A, Lee M, Li T, Smallwood N, Chiang JY, Hardwick JP, Moore DD, et al. (2014) All-trans-retinoic acid ameliorates hepatic steatosis in mice by a novel transcriptional cascade. Hepatology 59, 1750–60. [PubMed: 24038081]

(38). Shiota G (2005) Loss of function of retinoic acid in liver leads to steatohepatitis and liver tumor: A NASH animal model. Hepatol. Res 33, 155–60. [PubMed: 16202648]

(39). Sell S (2004) Stem cell origin of cancer and differentiation therapy. Critical reviews in oncology/hematology 51, 1–28. [PubMed: 15207251]

(40). Bryan M, Pulte ED, Toomey KC, Pliner L, Pavlick AC, Saunders T, and Wieder R (2011) A pilot phase II trial of all-trans retinoic acid (Vesanoid) and paclitaxel (Taxol) in patients with recurrent or metastatic breast cancer. Invest. New Drugs 29, 1482–7. [PubMed: 20596747]

(41). Gruenbaum Y, and Medalia O (2015) Lamins: the structure and protein complexes. Curr. Opin. Cell Biol 32, 7–12. [PubMed: 25460776]

(42). Buxboim A, Swift J, Irianto J, Spinler KR, Dingal PC, Athirasala A, Kao YR, Cho S, Harada T, Shin JW, et al. (2014) Matrix elasticity regulates lamin-A, C phosphorylation and turnover with feedback to actomyosin. Curr. Biol 24, 1909–17. [PubMed: 25127216]

(43). Hattinger CM, Vella S, Tavanti E, Fanelli M, Picci P, and Serra M (2016) Pharmacogenomics of second-line drugs used for treatment of unresponsive or relapsed osteosarcoma patients. Pharmacogenomics 17, 2097–2114. [PubMed: 27883291]

(44). Alkema NG, Wisman GB, van der Zee AG, van Vugt MA, and de Jong S (2016) Studying platinum sensitivity and resistance in high-grade serous ovarian cancer: Different models for different questions. Drug Resist. Updates 24, 55–69.

(45). Amini-Fazl MS, Mobedi H, and Barzin J (2014) Investigation of aqueous stability of taxol in different release media. Drug Dev. Ind. Pharm 40, 519–26. [PubMed: 23594296]

(46). Avis I, Mathias A, Unsworth EJ, Miller MJ, Cuttitta F, Mulshine JL, and Jakowlew SB (1995) Analysis of small cell lung cancer cell growth inhibition by 13-cis-retinoic acid: importance of bioavailability. Cell growth & differentiation: the molecular biology journal of the American Association for Cancer Research 6, 485–92. [PubMed: 7647031]

(47). Ueda J, Yoshida H, Mamada Y, Taniai N, Mineta S, Yoshioka M, Kawano Y, Furuki H, Koizumi K, and Uchida E (2012) Surgical resection of solitary metastatic liver tumor arising from lung cancer: a case series. Hepato-Gastroenterology 59, 2307–9. [PubMed: 22389293]

(48). Tamura T, Kurishima K, Nakazawa K, Kagohashi K, Ishikawa H, Satoh H, and Hizawa N (2015) Specific organ metastases and survival in metastatic non-small-cell lung cancer. Mol. Clin. Oncol 3, 217–221. [PubMed: 25469298]

(49). Chaffer CL, and Weinberg RA (2011) A perspective on cancer cell metastasis. Science 331, 1559–64. [PubMed: 21436443]

(50). Irianto J, Xia Y, Pfeifer CR, Athirasala A, Ji J, Alvey C, Tewari M, Bennett RR, Harding SM, Liu AJ, et al. (2017) DNA Damage Follows Repair Factor Depletion and Portends Genome Variation in Cancer Cells after Pore Migration. Curr. Biol 27, 210–223. [PubMed: 27989676]

(51). Ivanovska IL, Swift J, Spinler K, Dingal D, Cho S, and Discher DE (2017) Cross-linked matrix rigidity and soluble retinoids synergize in nuclear lamina regulation of stem cell differentiation. Mol. Biol. Cell 28, 2010–2022. [PubMed: 28566555]

(52). Shin JW, Spinler KR, Swift J, Chasis JA, Mohandas N, and Discher DE (2013) Lamins regulate cell trafficking and lineage maturation of adult human hematopoietic cells. Proc. Natl. Acad. Sci. U. S. A 110, 18892–7. [PubMed: 24191023]

(53). Gruz-Gibelli E, Chessel N, Allioux C, Marin P, Piotton F, Leuba G, Herrmann FR, and Savioz A (2016) The Vitamin A Derivative All-Trans Retinoic Acid Repairs Amyloid-beta-Induced Double-Strand Breaks in Neural Cells and in the Murine Neocortex. Neural Plast 2016, 1.

(54). Lock LL, Reyes CD, Zhang P, and Cui H (2016) Tuning Cellular Uptake of Molecular Probes by Rational Design of Their Assembly into Supramolecular Nanoprobes. J. Am. Chem. Soc 138, 3533–40. [PubMed: 26890853]

(55). Lee WP (1993) The role of reduced growth rate in the development of drug resistance of HOB1 lymphoma cells to vincristine. Cancer Lett 73, 105–11. [PubMed: 8221621]

(56). Cunningham JJ, Gatenby RA, and Brown JS (2011) Evolutionary dynamics in cancer therapy. Mol. Pharmaceutics 8, 2094–100.

(57). Jing YK, Wang L, Xia LJ, Chen GQ, Chen Z, Miller WH, and Waxman S (2001) Combined effect of all-trans retinoic acid and arsenic trioxide in acute promyelocytic leukemia cells in vitro and in vivo. Blood 97, 264–269. [PubMed: 11133770]

(58). El-Serag HB, Marrero JA, Rudolph L, and Reddy KR (2008) Diagnosis and treatment of hepatocellular carcinoma. Gastroenterology 134, 1752–63. [PubMed: 18471552]

(59). Nair PR, Karthick SA, Spinler KR, Vakili MR, Lavasanifar A, and Discher DE (2016) Filomicelles from aromatic diblock copolymers increase paclitaxel-induced tumor cell death and aneuploidy compared with aliphatic copolymers. Nanomedicine 11, 1551–69. [PubMed: 27177319]

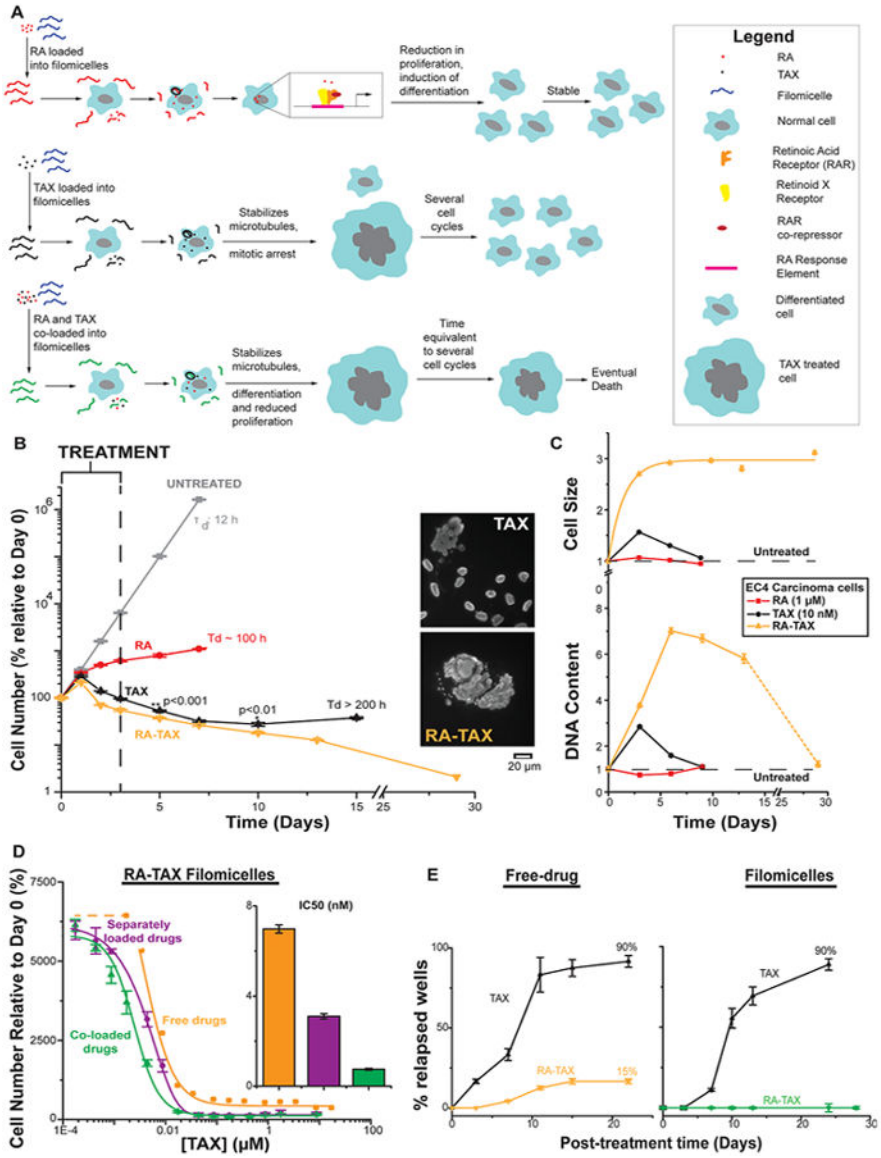

Figure 1.

(A) Schematic depicting effect of RA, TAX, and RA-TAX on cells after filomicelles release drugs. Only RA-TAX combination leads to durable effects. (B) Cells treated with RA consistently increase in number, consistent with RA not killing cells, just differentiating them. TAX treated cells decline in number initially (similar to initial tumor shrinkage), but cell death plateaus after a week when proliferating cell numbers overtake dying ones. RA and TAX treated cells, on the other hand, consistently decrease in number, indicating a more durable treatment. (C) Quantification of DNA content and cell size after drug treatment. DNA content increases for TAX and RA-TAX due to incomplete cell division; it decreases for RA due to a lower number of proliferating cells (and hence lower DNA replication before division). DNA content for cells treated with single drugs returns to normal after about 6 days (about 3 days after treatment), indicating the transient nature of single drugs, whereas DNA content for RA-TAX decreases much more slowly. Similarly, cell size for

single drugs returns to normal within 3 days, indicating the transient nature of single drugs. However, they remain consistently high for combination treatment. (D) Delivery systems with two payloads can be coloaded onto the same micelle or on separate filomicelles which are then mixed. At high concentrations, both are equally effective. However, at therapeutic concentrations (around IC50), coloaded filomicelles are 4 times more potent than separately loaded filomicelles (inset bar graph). (E) Most wells treated with TAX relapse (92%), the rate is much lower for RA-TAX treated wells (15%) 22 days post-treatment, indicating that 85% of wells exposed to RA-TAX die, which illustrates a much more durable treatment than the single drug. Loading TAX onto filomicelles does not alter relapse (89% of TAX treated wells experienced relapse), highlighting again the limitation of a single drug. The efficacy of RA-TAX was greatly improved via loading onto filomicelles, with no relapses in cells observed after 30 days.

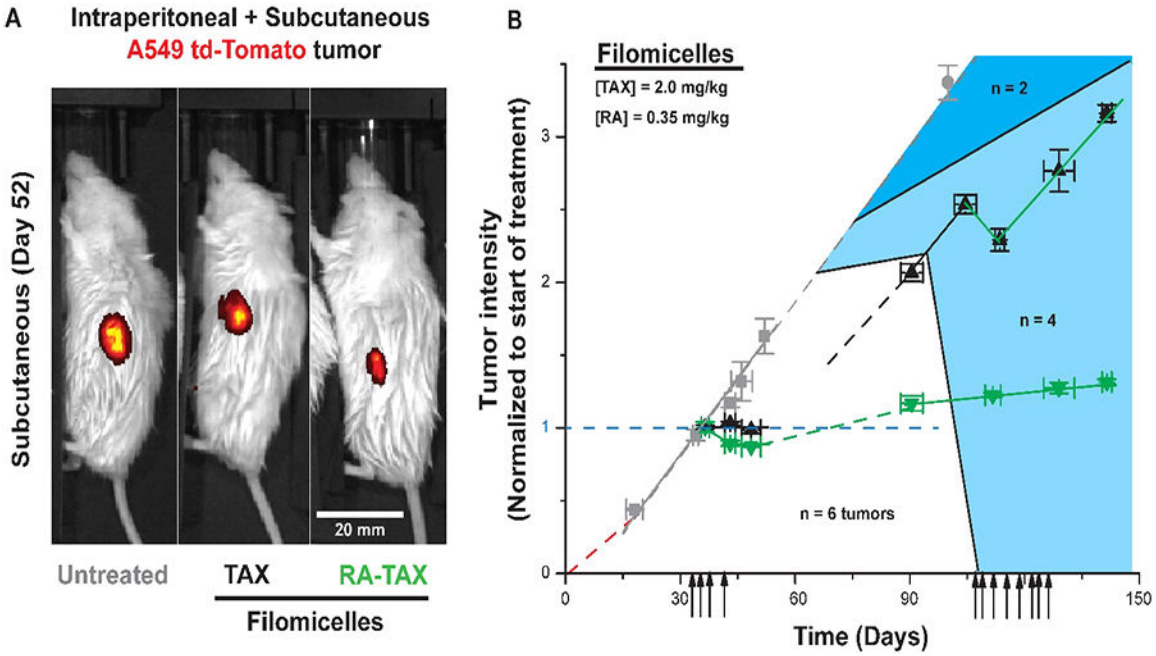

Figure 2.

(A) td-Tomato images of subcutaneous tumors on untreated, TAX and RA-TAX treated mice at day 52. RA-TAX treated mice had the smallest tumors and td-Tomato intensity. (B) Mice bearing A549 subcutaneous tumors were injected 4 times with single drug (TAX, black points) or combination (RA-TAX, green points) loaded into filomicelles. RA-TAX combination produced the most tumor shrinkage (30%) which remained shrunk for 20 days and grew slowly after that.

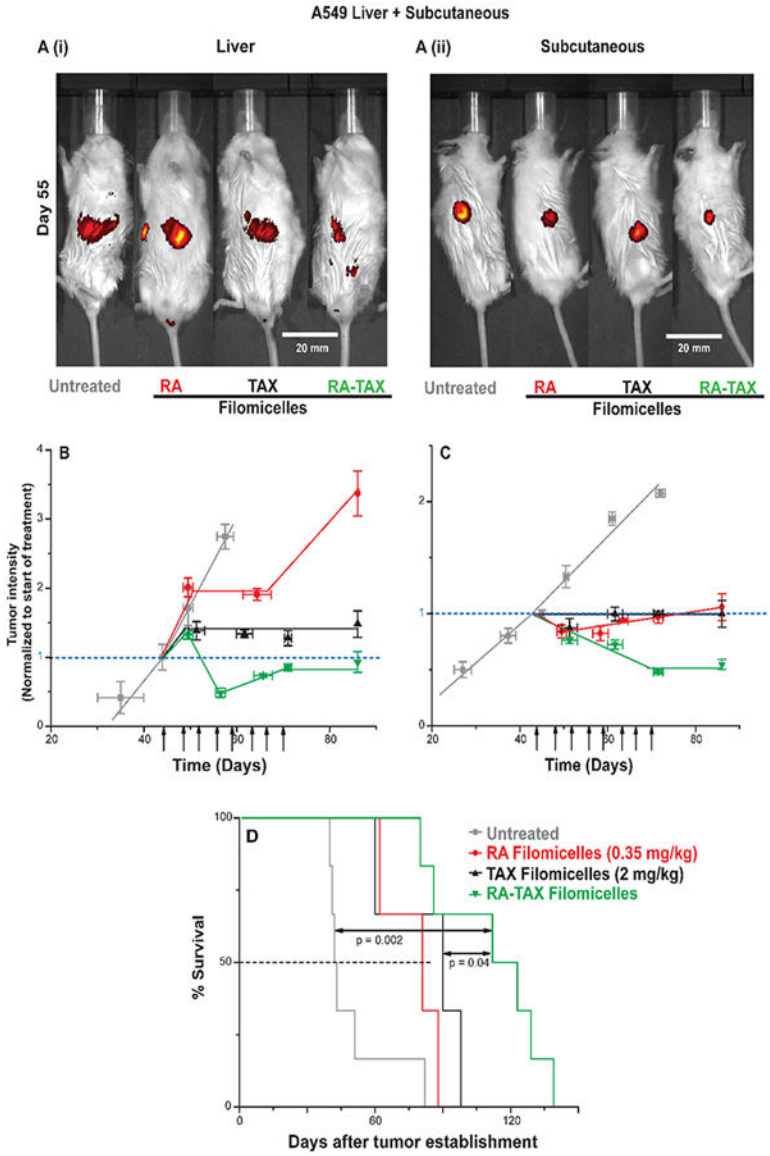

Figure 3.

(A) td-Tomato images of liver and subcutaneous tumors on untreated, RA, TAX, and RA-TAX treated mice at day 55. RA-TAX treated mice had the lowest td-Tomato intensity in both cases. (B) RA-TAX filomicelles were efficacious with orthotopic A549 liver tumors, shrinking and arresting the growth of tumors, while single drugs failed to do both. While TAX controlled the growth of tumors, those treated with RA continue to grow. (C) RA-TAX filomicelles shrunk subcutaneous A549 tumors by ~50%. Single drug controls arrest the growth of tumors 30 days from the start of the treatment. During the same time frame, untreated tumors more than double in size. (D) Kaplan−Meier curve showing significant prolonged survival of RA-TAX treated mice A549 liver and subcutaneous tumors.

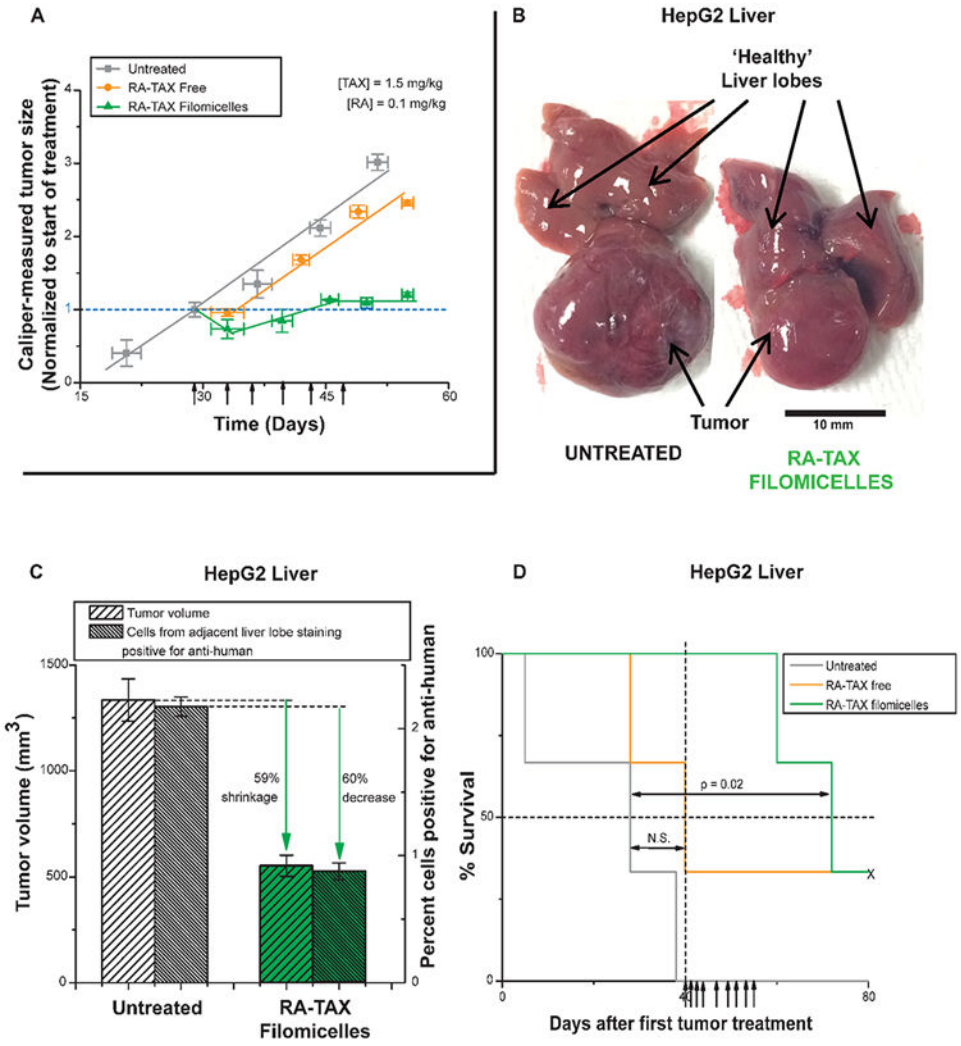

Figure 4.

(A) RA-TAX suppressed the growth of HepG2 subcutaneous tumors in vivo. Mice treated with RA-TAX filomicelles experienced 30% growth in tumors, while untreated tumors more than tripled in size during the same time frame. Free RA-TAX produced minimal retardation in tumor growth. (B) Orthotopic liver tumors established in vivo from HepG2 cells. RA-TAX treated tumors are 65% smaller than untreated tumors. (C) Quantification of liver tumor size from (B) and antihuman stain in adjacent liver lobe to identify number of HepG2 cells migrating. Quantification of cells staining positive is depicted in the bar graph. (D) Kaplan−Meier curve showing significant prolonged survival of RA-TAX treated mice with HepG2 liver tumors.

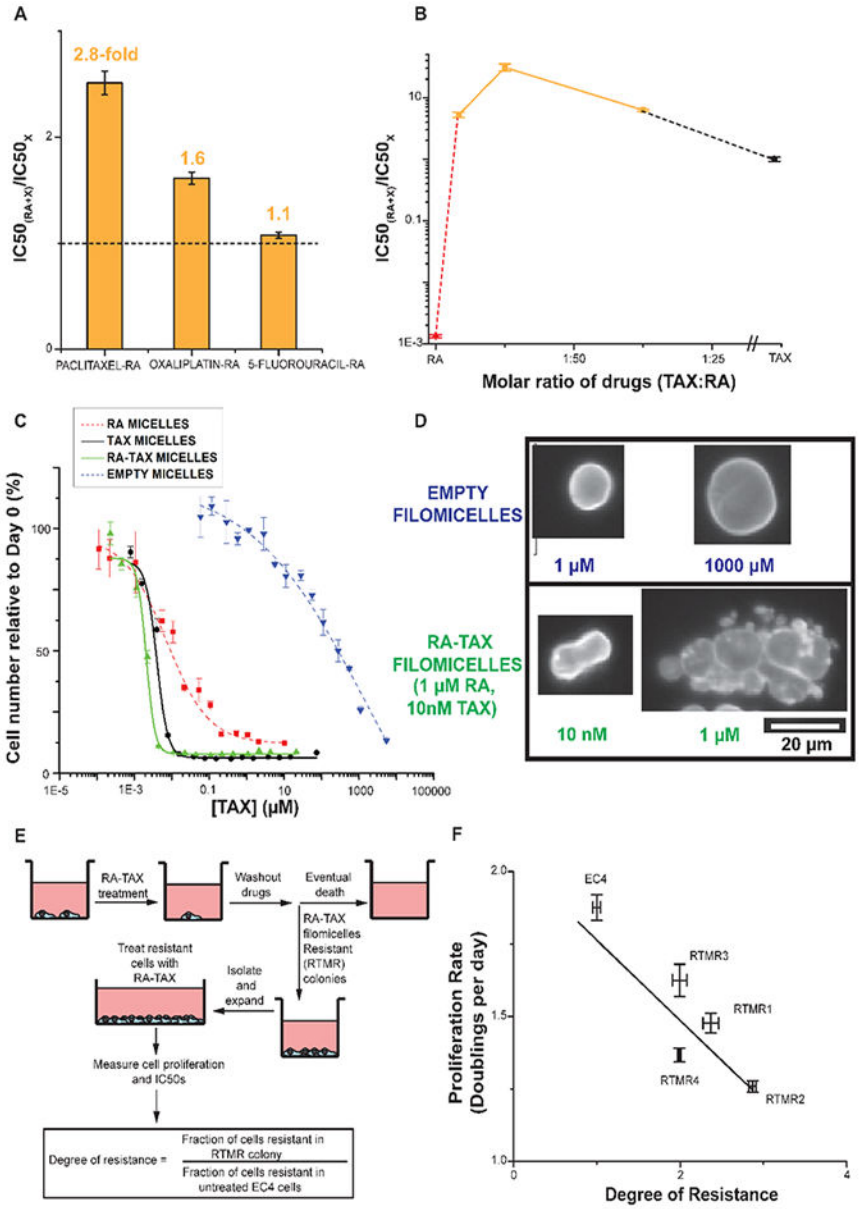

Figure 5.

(A) Bar graph representation of the fold change in IC50 with RA-drug combination. Combination of 5-fluorouracil shows negligible change in IC50, and oxaliplatin-RA showed a 1.6-fold change in IC50, signifying some synergy. However, combination of RA and Paclitaxel had a 2.5-fold reduced IC50 than parent chemotherapeutic (Paclitaxel), signifying maximum synergy among the three combinations and the best candidates for further experiments. (B) Molar ratio dictates improvement in IC50 with combination of TAX and RA, with 1:100 being optimal. (C) Testing of RA, TAX, and RA-TAX loaded filomicelles on EC4 mouse liver cancer cells. TAX (black) has a much lower IC50 than RA (red) as it induces apoptosis instead of arresting proliferation. However, the combination of RA-TAX is more effective than either drug alone, with its IC50 less than half of that for TAX. Empty filomicelles (blue curve) were inert at the desired concentrations. (D) Nuclei treated with

Paclitaxel (TAX) exhibit massive blebbed nuclei due to incomplete division (bottom). Untreated nuclei (top) in contrast are smooth and rounded. (E) Schematic depicting culture of resistant colonies arising after RA-TAX filomicelle treatment. (F) Plotting the proliferation rate against the degree of resistance gives an inverse relation, supporting the hypothesis that acquisition of drug-resistance occurs at the cost of proliferation.

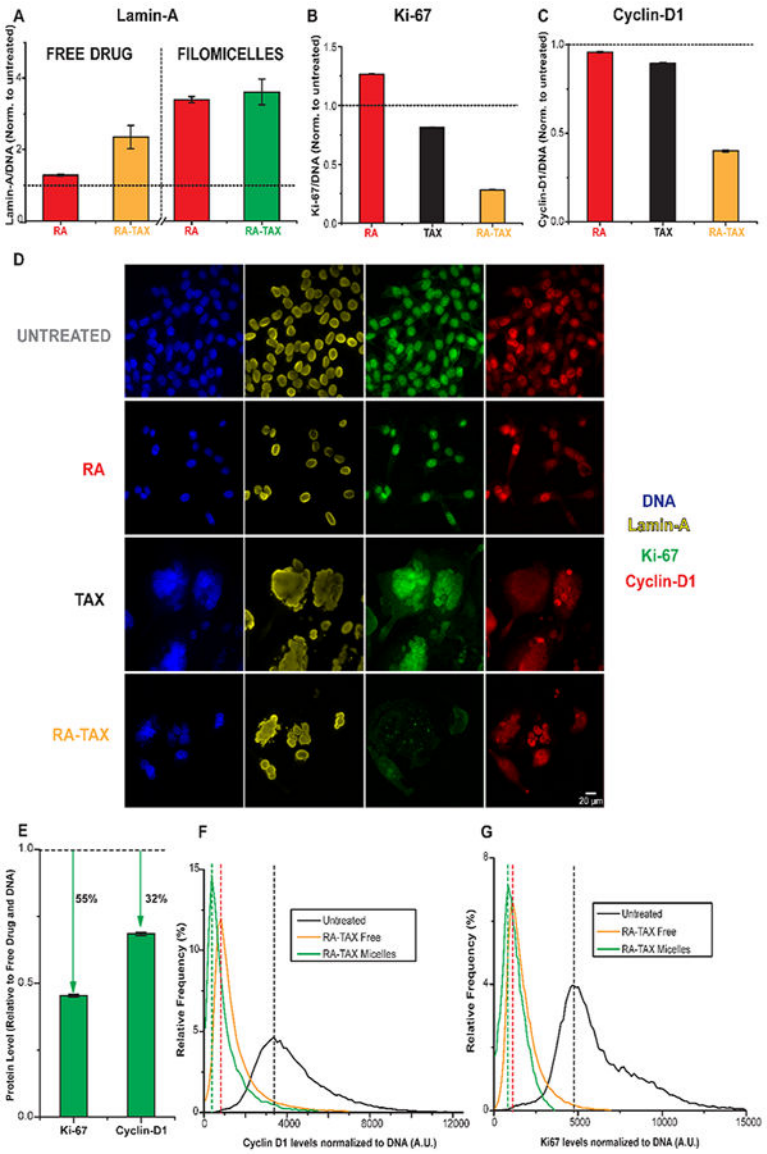

Figure 6.

(A) RA and TAX treated cells were found to have higher levels of lamin-A than untreated ones, suggesting differentiation. Lamin-A levels were higher for drugs delivered via nanocarriers than for free drugs. (B,C) RA-TAX treated cells have lower levels of and Cyclin-D1 than TAX or RA alone treated cells. The durability of RA-TAX combination might be explained by its inhibitory role on protein synthesis (via Ki-67) rather than regulation of cell cycle (CyclinD1). (D) Images (40× magnification) of cells treated with RA, TAX, and RA-TAX combination, as well as untreated. All groups except RA-TAX stain positive for Ki-67. Lamin-A is higher in RA-TAX treated cells. (E) Delivery of drugs via filomicelles has been proven to be superior to free drugs, and this mode further reduces levels of these two proteins, with Ki-67 levels being halved compared to free drug treated. (F,G) histogram of Ki-67 and Cyclin D1 levels after treatment with various drugs loaded

onto filomicelles. The fractions of cells null for these proteins progressively increases from no treatment to free drug to micellar drug delivery.

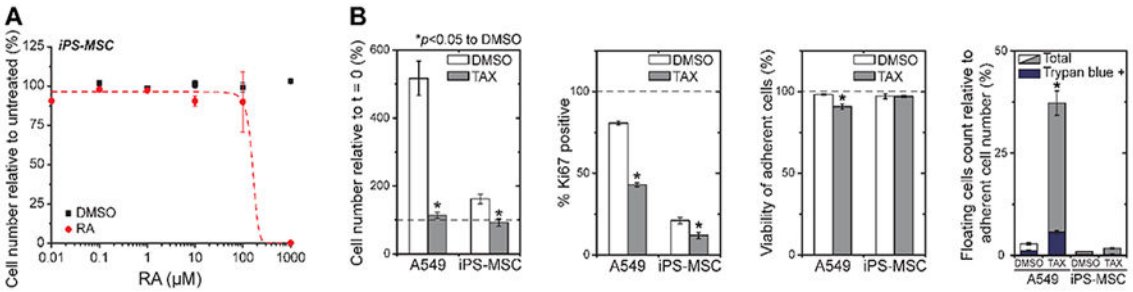

Figure 7.

(A) Quantifying RA effect on human derived induced pluripotent stem cells that were differentiated into mesenchymal stem cell lineage (iPS-MSCs). (B) Exposure to 10 nM TAX for 72 h blocks proliferation of both A549s and iPS-MSCs, as indicated by the decrease in cell number and proportion of Ki67 positive cells. In addition to the floating cells count, cell viability was also quantified by live/dead staining using Calcein-AM (live) and Ethidium Homodimer (dead). After the 10 nM TAX treatment, viability of the A549s is clearly more compromised (*$p < 0.05$ against DMSO).